Expression of SARS-CoV-2 Spike Protein (SP) and ACE2 via Lentiviral Vectors (LVs) to Target Glioblastoma (GBM): *In Vitro* Model for Viral-Mediated Fusogenic Therapy and Tumor Suppression

By:

Kimball Sheehan, Bryn Lafferty, Ashley Hemp, and Furman Wall
University of Virginia, Department of Biomedical Engineering Spring 2025

Faculty Advisor
Benjamin Purow, Department of Neurology

Word Count: 5277
Number of Figures: 8
Number of Tables: 0
Number of Equations: 0
Number of Supplements: 4
Number of References: 26

Approved: Benjamin Purow Date: April 28, 2025

Expression of SARS-CoV-2 Spike Protein (SP) and ACE2 via Lentiviral Vectors (LVs) to Target Glioblastoma (GBM): *In Vitro* Model for Viral-Mediated Fusogenic Therapy and Tumor Suppression

Kimball Sheehan[a]. Bryn Lafferty[a]. Ashley Hemp[a]. Furman Wall[a]. Yunge Zhao[b]. Benjamin Purow[b,1].

[a] University of Virginia Department of Biomedical Engineering, Undergraduate
[b] University of Department of Neurology
[1] Correspondence: Benjamin Purow

Abstract

Glioblastoma (GBM) is a highly aggressive and incurable brain cancer characterized by poor drug delivery across the blood-brain barrier (BBB) and resistance to conventional therapies. To address these limitations, a novel fusogenic therapeutic strategy has been proposed and developed that leverages the SARS-CoV-2 spike protein (SP) and ACE2 receptor to induce syncytia formation and stimulate anti-tumor immune responses within the tumor microenvironment (TME). This approach should promote immunogenic cell death and improve treatment efficacy through viral protein-mediated cell-cell fusion.

Experimental models, including *in vitro* experiments and assays, were employed to investigate the effects of SP and ACE2-induced fusion on GBM cells. Human (U251) and mouse (CT2A) GBM cell lines were engineered using lentiviral vectors (LVs) to express control (CV, control virus), SP, ACE2, or SP+ACE2. Stable U251 cell lines were developed and assessed for syncytia formation using DAPI staining and fluorescence microscopy, while cytotoxicity and cell viability were evaluated via Nano-Glo assays in luciferase-expressing cells under continuous expression regimens with varying SP and ACE2 ratios. Experimental data informed the development of a MATLAB-based computational model to predict GBM tumor response to varying SP and ACE2 expression ratios.

Results demonstrate the feasibility of this experimental framework and highlight its potential to model and modulate immune responses in GBM. Limitations include the use of an *in vitro*-only model and the lack of direct analysis of immune response markers. Future directions involve characterizing cytokine signaling using complementary assays, optimizing fusion efficiency, and expanding computational modeling to better predict therapeutic outcomes. This multidisciplinary approach, which integrates virology, immunology, and computational modeling, may inform personalized immunotherapeutic strategies and support broader applications of regulated viral protein expression in oncology.

Keywords: Glioblastoma (GBM), blood-brain barrier (BBB), tumor microenvironment (TME), spike protein (SP), ACE2 receptor, lentiviral vectors (LVs), fusogenic therapy, syncytia formation.

Introduction

Background of Glioblastoma

Glioblastoma (GBM), a World Health Organization (WHO) grade IV glioma, represents the most common and aggressive primary malignant brain tumor in adults, accounting for approximately 47.7% of central nervous system malignancies.[1] The annual incidence rate in the United States is 3.19 per 100,000, with a notably higher incidence among males, who are affected at a rate 1.6 times greater than females. The prognosis for GBM is exceptionally poor, with a median survival of only 16 months after diagnosis, and fewer than 5% of patients survive beyond five years post-diagnosis.[2,3] This outcome is largely due to GBM's rapid proliferation, resistance to current therapies, and highly invasive nature, which allows tumor cells to infiltrate healthy brain parenchyma–the functional tissue of the brain–complicating surgical resection and impeding effective targeting by chemotherapeutic agents.[4] Additionally, GBM's distinct tumor microenvironment (TME) and frequent therapeutic resistance contribute to its high recurrence rate, which further diminishes treatment outcomes. There is a substantial clinical need for new therapeutic modalities, as current treatments including surgery, radiation, and chemotherapy primarily serve to delay progression rather than provide a cure. These interventions are limited by factors such as the blood-brain barrier (BBB), which restricts drug delivery, and often result in neurological complications. Common issues include seizures, mood changes, memory problems, functional decline, depression, increased risk of infection, bleeding, and tumor recurrence.[5,6]

Gaps in Current Treatment

Standard GBM treatment typically includes a combination of surgical resection, radiation, and chemotherapy.[7] While these methods may delay progression, they do not prevent recurrence and always fail to fully eradicate the tumor. Treatments targeting GBM are constrained by the BBB, which prevents effective drug delivery to the tumor site. Compounding these challenges, GBM treatments often impact essential brain functions, leading to side effects like mood changes, memory deficits, and diminished ability to perform daily activities. GBM patients often face tumor recurrence and severe complications, including increased risk of infection and bleeding, which further diminish the quality of life and survival outcomes.[8] Immunotherapy and targeted therapy approaches are being explored but have shown limited efficacy due to GBM's unique TME, which impedes immune cell infiltration and prevents a sustained immune response. Therefore, there is a critical need to develop new therapeutic strategies that can specifically target GBM cells while enhancing immune response and minimizing side effects.

The current standard of care for GBM is chemotherapy and radiation, which follow maximal surgical resection (Figure 1).[9] The main goal of surgery is to remove as much of the tumor as possible; however, the GBM infiltrates normal tissue, meaning radiation and chemotherapy must also be used to kill the majority of the remaining tumor cells. Surgery involves reducing the overall tumor volume when relatively safe to do so. After the wound has healed, radiation therapy can begin. Radiation selectively kills the tumor cells that remain following surgery and those that infiltrate the normal brain parenchyma. Radiation treatments involve 10-30 sessions of standard-dose fractions of radiation that target the tumor site.[9] Chemotherapy initially consists of the drug temozolomide, an alkylating agent that slows the growth of cancer cells in the body by depositing methyl groups on DNA guanine bases.[10] Stereotactic radiosurgery (SRS) is occasionally used in GBM management,

primarily for small, well-defined recurrences. It delivers precise, high-dose radiation to targeted areas while minimizing exposure to adjacent critical structures.[11] Despite advances in these multidisciplinary treatment methods, most patients experience tumor progression, with the median survival rate being less than 16 months.[12] Current GBM treatments are inadequate, highlighting the urgent clinical need for alternative therapeutic approaches. New treatment modalities must improve survival, patient quality of life, and decrease complications.

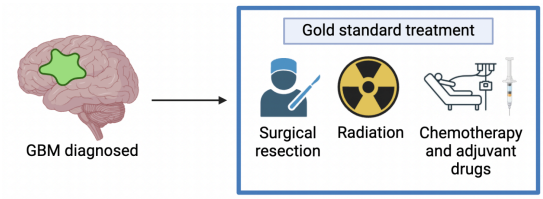

Figure 1. Current gold-standard treatments for GBM include surgery, radiation, and chemotherapy.

Overview of Solution and Prior Work

A new area of research for GBM treatment relies on modifying the gene expression of tumor cells. Genetic modification is particularly useful because it can give insight into the modified gene's role and can allow for fluorescent marking.[13] Transfection of GBM cells with plasmids is ineffective.[14] However, lentiviral gene delivery with vectors has been used for stable transduction of GBM cells.[13] LVs have emerged as a leading platform for gene delivery due to their ability to stably integrate into the host genome, enabling long-term gene expression. The genome of LVs is reverse-transcribed and then integrated into the host cell's genome. The most studied virus has been Human Immunodeficiency Virus type 1 (HIV-1) lentivirus. Lentiviruses have a highly improved safety profile and can be used to efficiently transfer genes.[15] Lentiviruses are of particular interest to cancer researchers due to their continuous gene expression following incorporation into the host genome. LVs have been widely used in GBM research due to their stability and resistance to genetic mutations compared to gammaretroviral vectors.[15] Additionally, LVs have numerous advantages over other gene delivery mechanisms: LVs can transduce both dividing and non-dividing cells, efficiently deliver genes to primary and stem cells, and integrate their genome into the host DNA, resulting in a safe and persistent gene expression.[15] Thus, the application of LVs for GBM treatments should be further investigated due to its novel and significant clinical potential. LVs have been investigated for cell and gene therapy, but research beyond that is limited. LVs have been used to deliver suicide genes such as HSV1-tk, which activates phosphorylation of ganciclovir, resulting in the cessation of DNA replication and cell death.[15] This strategy was shown to significantly reduce GBM tumor volume.[16] Some recent studies have investigated the effects of the SARS-CoV-2 virus or vaccine on cancer cell growth. One study found that vaccines for the SARS-CoV-2 virus inhibited cervical cancer cell growth.[17] The virus itself causes endogenous production of the virus SP, resulting in an increased host immune response. Wilson et al. found that the SP inhibited the proliferation of SiHa cancer cells with an up-regulation of anti-proliferative molecule p53 and induced apoptosis of SiHa cells with an increased expression of tumor necrosis factor apoptosis-inducing ligand (TRAIL) cytokine molecule. Another study investigated the effects of SARS-CoV-2 SP on prostate cancer cells. SP inhibited the proliferation and promoted apoptosis of LNCaP prostate cancer cells.[18] Johnson et al. found that SP inhibits the growth of prostate cancer via down-regulation of cyclin-dependent kinase 4 (CDK4) and up-regulation of pro-apoptotic molecule Fas ligand (FasL). There is increased expression of ACE2 receptors in the prostate epithelium,

testes, and kidneys.[19] Thus, given that SP preferentially binds ACE2 receptors, these areas were ideal targets for treatment with SP. More studies investigating the effect of SARS-CoV-2 SP on cancer cell proliferation and apoptosis are required to draw more conclusions about the potential effects in human cancer models.

Relevance and Broader Impact

This project introduces a novel therapeutic approach that utilizes the SARS-CoV-2 SP and ACE2 receptor to trigger syncytia, or cell fusions, in GBM cells, aiming to directly induce cell death and stimulate syncytia formation (Figure 2). This fusogenic therapy could address major limitations of current GBM treatments by creating an immune-activating environment within the tumor, potentially reducing the need for therapeutic agents to cross the BBB and limiting off-target effects

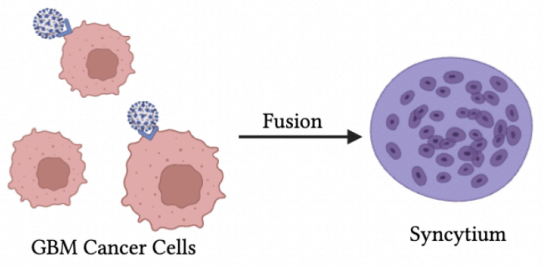

Figure 2. Syncytia formation driven by SARS-CoV-2 spike protein and ACE2 receptor fusion.

The syncytia formation driven by the SARS-CoV-2 SP and ACE2 receptor may offer a potential strategy for inducing tumor cell death, although further work is needed to determine selectivity and minimize effects on surrounding brain tissue. This approach could also enhance immune cell recruitment to the tumor site, fostering a pro-inflammatory environment that boosts the immune system's recognition and attacks GBM cells more effectively. Syncytia not only contribute to direct tumor cell death but also have the potential to enhance immune cell recruitment by exposing tumor antigens and inducing danger signals.[20] This dual functionality supports their relevance in immunotherapeutic strategies.

In addition, this project will develop a MATLAB-based predictive model to evaluate the response following treatment with SARS-CoV-2 SP and ACE2 receptor expression in GBM. The model aims to simulate how varying treatment conditions influence cell viability and syncytia formation, enabling optimization of therapeutic regimens that enhance immune activation while minimizing toxicity to surrounding healthy tissue. By guiding hypotheses about expression timing and dosage, this model may help inform future strategies to optimize GBM therapies based on immune dynamics. Ultimately, this research seeks to establish a fusogenic treatment framework that maximizes SP-mediated tumor cell fusion and immune engagement while minimizing off-target cytotoxicity. Beyond GBM, this project could serve as a foundational model for adapting fusogenic therapies to other therapy-resistant solid tumors.

Results

Stable Cell Line Development

To enable the subsequent selection and generation of stable cell lines with lentivirus also bearing a puromycin resistance gene–allowing for expression of SP, ACE2, or both–varying puromycin concentrations were tested to verify the optimal dosage for the human GBM cell lines U251 and U87. A puromycin kill curve was first conducted to identify the minimal effective concentration necessary to eliminate non-transduced cells while minimizing off-target toxicity to successfully transduced cell lines. Cells were plated in 24-well plates and allowed to proliferate until reaching 60–70% confluency, at which point media containing puromycin was added and replaced every 48 hours.

Lentiviral transduction ratios were selected based on the multiplicity of infection (MOI), which reflects the number of viral particles per target cell. After transduction, puromycin was added to the media to select for cells that had successfully incorporated the vector, as each construct contained a puromycin resistance gene. The U251 cell line concentration was successfully determined after two rounds of testing, whereas the U87 line required additional optimization and further kill curve experiments due to less consistent results.

Parental U251 cells were treated with a range of puromycin concentrations over 5 to 7 days, starting from 0 to 20 µg/mL, followed by a refined range of 0 to 5 µg/mL in two-fold increments. This process was completed to determine the lowest concentration that achieved complete cell death in transduced cells while allowing survival of successfully transduced cell populations. Cell viability was monitored daily via inverted light microscopy, and cell confluency was used as a proxy for survival. Complete cell death of the U251 cells was observed at a concentration of 0.625 µg/mL. This concentration was thus the optimal concentration for future stably transduced populations after conducting a crystal violet cell viability staining assay (Figure 3).

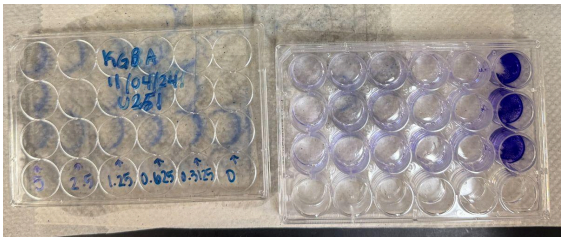

Figure 3. Results from the kill curve of puromycin on U251 GBM cells. In the final experiment, qualitative analysis using microscopy informed the concentration of puromycin needed for the U251 cell line to make the stable cells transduced with SARS-CoV-2 spike and ACE2 receptor proteins.

To evaluate the effects of SP and ACE2 expression on GBM cells, stable cell lines were first established and assessed for syncytia formation and cell viability across multiple expression ratios. Transduced U251 cell lines (SP, ACE2, SP+ACE2, and CV) were established by adding the LVs, followed by the optimal puromycin concentration determined using the methods above. These lines were maintained under continuous puromycin selection and subsequently validated via fluorescence non-inverted microscopy imaging and staining for downstream fusion analysis and viability assays. These stable lines serve as a foundational tool for reproducible testing and will support longitudinal studies examining gene expression stability, fusion consistency, and downstream immunologic markers.

In Vitro Viability and Fluorescence Assays

A series of *in vitro* assays were performed to evaluate the impact of the Wuhan strain of SARS-CoV-2 SP and ACE2 co-expression on GBM cells. Fusion phenotypes were assessed 48–72 hours post-combination to allow for sufficient protein expression. Fluorescence imaging revealed increased syncytia formation in conditions where both SP and elevated levels of ACE2 were expressed (Figure 4). Notably, co-expression of SP and ACE2 led to multinucleated giant cells characteristic of syncytia, while minimal fusion was observed in groups expressing either SP or ACE2 alone. These cells were generally larger, with shared cytoplasm, and contained ≥3 distinct nuclei, a hallmark of SP-mediated fusion.

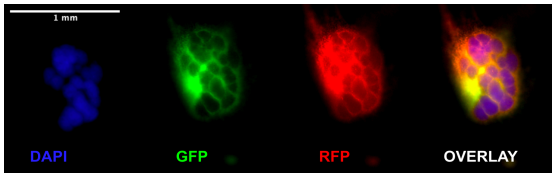

Figure 4. Fluorescence imaging of U251 stable cell lines co-expressing SP (RFP, red) and ACE2 (GFP, green), with nuclei stained by DAPI (blue). The distinct fluorescence signals confirm successful uptake and expression of both proteins. The image demonstrates syncytia formation, indicative of cell fusion, as well as dispersed cells showing co-expression of SP and ACE2. Images were acquired at 40X magnification.

Initial viability assays using Nano-Glo® luciferase were conducted on CT2A-SP H3 and H6 subtype cell lines, a parental CT2A line, and U251-luciferase cells. The results are shown in Figure 5. In the CT2A-SP H3 subtype cells, a statistically significant decrease in luminescence, which was used as a proxy for cell viability, was observed in the 2:1 and 1:1 ratio conditions. However, these statistically significant findings were limited to the CT2A-SP H3 subtype. The CT2A-SP H6 subtype showed no significant differences, which suggests potential variability in SP expression or fusion efficiency between subtypes. Immunoblotting for SP expression in both H3 and H6 subtypes may be necessary to confirm if the variability arises from differential transgene expression levels. Moreover, U251-luciferase cells are human-derived, while CT2A is a murine cell line. Thus, interspecies interactions may have contributed to biological heterogeneity, inconsistent results, and reduced interpretability. Based on these preliminary results, the experimental design was refined to improve biological species homogeneity by replacing CT2A with the human-derived U251 cell lines expressing SP and SP+ACE2. This will allow for alignment of the species origin across cell models and enable more consistent fusion and viability comparisons.

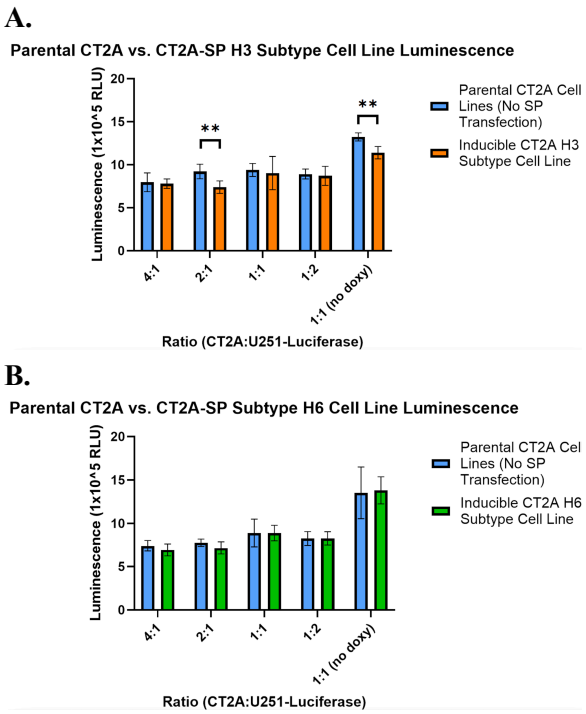

Figure 5. Luminescence readings for the combination of human GBM U251-luciferase cell lines with CT2A mouse cell lines, expressing **(A)** H3 or **(B)** H6 SP subtypes. Statistical significance was determined using a two-tailed unpaired t-test ($p < 0.01$, denoted by **). Error bars represent ± standard deviation.

To mitigate species-specific interactions and variability, all subsequent viability assays used human-derived U251 cells exclusively. These cells were engineered to stably express luciferase and co-transduced with SP, ACE2, or CV constructs at various MOI ratios.

Subsequent assays with U251 cells demonstrated a significant decrease in luminescence signal when SP was expressed, indicating reduced viability of U251-luciferase cells in the presence of SP and ACE2-mediated fusion. Quantified luminescence values showed statistically significant reductions in cell viability in groups expressing SP alone (1:1) and in SP+ACE2 combinations (4:1) when compared to controls ($p < 0.05$ and $p < 0.01$, respectively), as determined by two-tailed unpaired t-tests (Figure 6). The data support the hypothesis that SP and ACE2 interactions drive syncytia formation and reduce overall cell viability.

A.

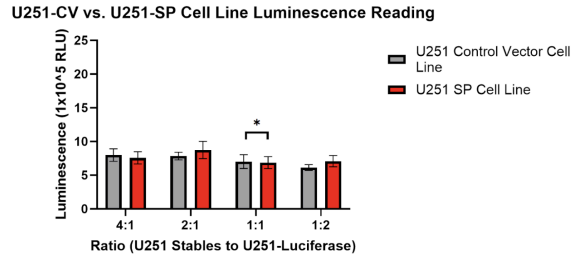

B.

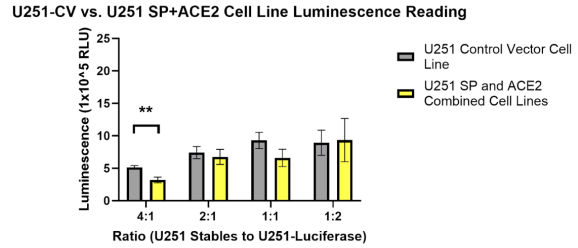

Figure 6. Luminescence readings for the combination of U251 cell lines, either expressing CV or SP in varying ratios. Statistical significance was determined using a two-tailed unpaired t-test ($p < 0.05$ denoted by *, $p < 0.01$ denoted by **). Error bars represent ± standard deviation.

While reductions in luminescence were observed for most of the other ratios, the differences did not reach statistical significance. This may be due to threshold effects in fusion dynamics or variability in transgene expression levels. The consistent trend of decreased viability in the SP+ACE2 groups compared to the CV group suggests the importance of ratios in influencing the effect of fusion on the cells. This suggests a synergistic cytopathic effect, where both viral proteins are required for maximal fusion and consequent cell death. These results demonstrated the effectiveness of syncytia formation in inducing a decrease in GBM cell viability. Also, the results validated that an all-human U251 model is more effective than the murine-human mixed model to study SP-ACE2-mediated cytotoxicity.

Computational Model

To complement the experimental observations, a computational model was constructed to simulate the kinetics of SP-ACE2-mediated fusion in GBM populations. Using a logistic function informed by Nano-Glo® viability results, the model simulated the relationship between viral expression ratios and cell survival. The model was coded in MATLAB. A few key assumptions had to be established. SP and ACE2 expression levels remain constant per cell, and each fusion event results in the death of both participating cells post-syncytia formation. Also, the model assumed that once the cells die due to fusion, they cannot recover or re-enter the viable cell population. Thus, cell death was treated as irreversible, and no regeneration mechanisms were included in the system. It was also assumed that the GBM cells initially proliferated according to a logistic growth model and that the anti-tumor response of the syncytia is delayed by 3 days. Literature-derived parameters were used to approximate immune response onset (t_{delay}), rate of syncytia formation (k_f) and degradation(k_{deg}), and cell death kinetics (k_d).[21 22]

The model simulated a hypothetical *in vitro* experiment in which all starting cell numbers were constant, allowing direct comparison across treatment groups. Simulated conditions included the following viral ratios of SP:ACE2:CV, including 6:2:0, 4:4:0, 4:2:2, 2:4:2, and 2:2:4, each designed to test a range of fusion-competent and fusion-deficient conditions. The logistic curve predicted maximal viability loss in the 6:2:0 and 4:4:0 groups, aligning with experimental trends and supporting the hypothesis that increasing SP and ACE2 levels synergistically promote fusion-driven cytotoxicity (Figure 7).

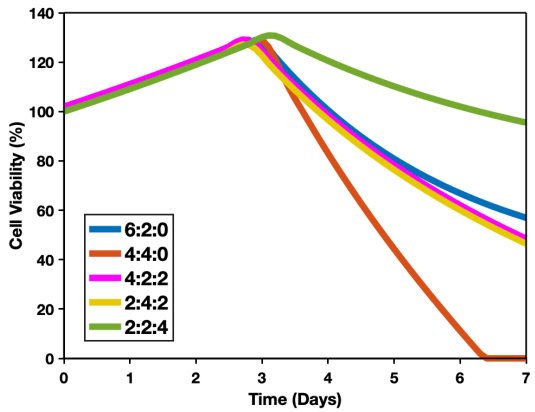

Figure 7. Theoretical model of percent cell viability of human U251 GBM luciferase cells in response to varying SP: ACE2:CV expression ratios over a 7-day period. The model incorporates logistic growth to account for cell proliferation and a 3-day delay to approximate the lag between syncytia formation and cell death. Legend indicates ratios in SP:ACE2:CV order. *(Note: cell viability is relative to the initial cell count.)*

Model outputs suggested that viability sharply declines beyond a critical SP:ACE2 threshold, reflecting a non-linear response where syncytia formation accelerates cell loss. In contrast, conditions with higher proportions of control virus (e.g., 2:2:4) showed relatively more preserved viability. These simulations provided a useful framework to predict fusion dynamics and to guide future optimization of viral ratios *in vivo*. Moreover, the model allows for hypothesis testing beyond experimental feasibility by simulating therapeutic scenarios that may be difficult to evaluate *in vitro*. This includes projecting fusion efficacy under varying expression timelines or dose-dependent effects of viral constructs, which can inform future experimental design.

A second model focusing solely on fusion frequency was developed to validate syncytia trends independently of viability. The model was constructed for percent syncytia formation (Figure 8). The model assumes syncytia formation is a binary and saturable reaction process, meaning fusion only occurs between cells expressing SP and ACE2. Once fusion occurs, both participating cells are removed from the viable population. The fusion rate follows a Michaelis-Menten saturation function, which reflects biological limits on cell fusion. Syncytium was assumed to degrade over time at a constant rate. The remaining assumptions carry over from the previous model.

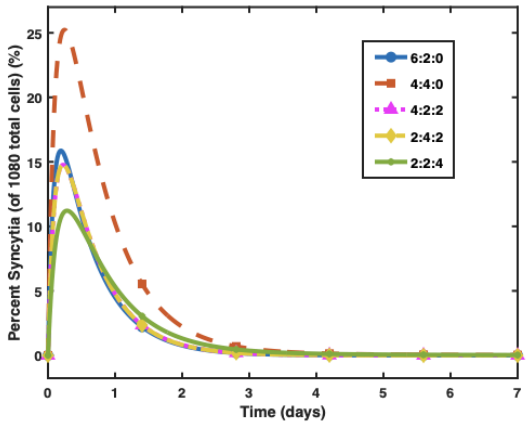

Figure 8. Theoretical model of percent syncytia formation from different combination ratios of SP:ACE2:CV in U251 stable cells over a 7-day period. Legend indicates ratios in SP:ACE2:CV order.

This syncytia prediction model indicates the highest rate of fusion in the 4:4:0 ratio of SP:ACE2:CV. This aligns with the group's hypothesis that higher and equally represented amounts of both the SP and ACE2 receptor translate to increased syncytia formation due to each component's dependency on the other. Although the model captures key biological dynamics, it does not currently account for heterogeneity in transduction efficiency or variable fusion competency, both of which may influence outcomes *in vivo*. Future iterations could include cell-to-cell variation elements or spatial modeling to refine predictive accuracy.

Discussion

Significance

This study establishes the feasibility of utilizing viral protein-mediated cell-cell fusion as a novel therapeutic strategy for GBM, a cancer characterized by its resistance to conventional and immune-based treatments. By engineering GBM cells to express the Wuhan

strain SARS-CoV-2 SP, the ACE2 receptor, or both, syncytia formation was reliably induced *in vitro* using human U251 cell lines. This fusion process results in significant reductions in cell viability and, *in vivo,* may also offer a promising strategy for initiating immunogenic cell death, potentially enhancing immune cell recruitment and priming an anti-tumor response within the TME.

While the current work does not yet address challenges such as BBB permeability or tumor heterogeneity and complexity, it provides essential proof-of-concept data using a human-derived *in vitro* model system. The integration of stable lentiviral expression, luciferase-based viability assays, and predictive computational modeling enables robust, quantitative analysis of fusion kinetics and cell death dynamics. This work establishes a foundational framework for future investigations into fusogenic therapies, which should aim to optimize fusion efficiency, elucidate immune responses, and explore delivery strategies.

By providing mechanistic insights into viral fusion as a therapeutic modality, this study offers new direction in GBM research. It also lays the groundwork for future *in vivo* studies aimed at optimizing fusion efficiency, characterizing immune activation, and developing clinically relevant delivery strategies. Ultimately, this interdisciplinary platform could inform new therapeutic paradigms in immuno-oncology and will target tumor cells through a unique, engineered mechanism of action. This work also lays the groundwork for future studies that explore how fusogenic therapies can be integrated with immune monitoring or combinatorial treatments. As GBM remains a highly treatment-resistant tumor, having a flexible modeling platform allows for iterative testing of next-generation strategies.

Innovation

This study presents a novel therapeutic strategy that harnesses the fusogenic properties of the SARS-CoV-2 SP and ACE2 receptor to selectively induce syncytia formation and cytotoxicity in GBM cells. Rather than relying on conventional cytotoxic agents or immune checkpoint inhibitors, this approach initiates direct tumor cell fusion as a mechanism of cytotoxicity. This fusion-based strategy offers a distinct therapeutic modality that functions independently of T cell activation, which may be beneficial in the context of GBM's immunologically "cold" TME.[23]

Key innovations of the study include the development of stably transduced human U251 cell lines expressing SP or ACE2, which enable consistent and reproducible modeling of fusion interactions. Quantitative viability assays based on luminescence allow for real-time monitoring of fusion-associated cytotoxicity across varied cell ratios. The inclusion of a computational model further enhances the platform by providing predictive insights into syncytia formation dynamics and enabling optimization of experimental conditions.

To our knowledge, this is the first application of a SARS-CoV-2–derived viral fusion system in a human GBM context, and one of the first to explore its use as a therapeutic tool in solid tumors. This work introduces a new paradigm in cancer research by repurposing viral fusion machinery to disrupt tumor integrity and promote tumor-selective immune activation. Together, this work highlights the utility of viral-based fusogenic approaches as a modular platform for engineering tumor-specific cell death, with potential applications beyond GBM.

Challenges and Limitations

One of the most significant challenges faced in this project was determining the appropriate puromycin concentration required to select for stable expression in LV-transduced

GBM cells. This process had no established protocols in the literature for the specific cell lines (U251 and U87) and constructs used. Therefore, kill curves were established and conducted via a trial-and-error process, which was time-consuming given each cell line's significantly different sensitivity and response to puromycin. Additionally, there was uncertainty as to whether the cells would successfully uptake and express the LV, particularly in the U87 cell line, where most attempts at transduction were unsuccessful. These limitations created delays in the generation of stable cell lines and added variability to early experiments. Future work will require further optimization of transduction conditions and careful validation of construct expression to ensure consistency across cell populations.

In the *in vitro* model, syncytia formation and direct GBM cell killing were studied using GBM cell lines U251 and U87, which were convenient and well-characterized. One limitation of the *in vitro* model was that the cell lines do not fully replicate the complexity of patient-derived GBM tumors. These human GBM cells lack key features such as tumor heterogeneity, immune interactions, the BBB, the TME, and tumor-initiating cell populations. Additionally, the immune response was inferred from morphological syncytia analysis and cell viability assays, rather than from functional immune readouts. Co-culturing with immune cells or using more physiologically relevant 3D culture systems would help address these limitations in future studies.

The computational model was developed to simulate syncytia formation and GBM U251 cell viability in response to different SP:ACE2:CV ratios using a system of ordinary differential equations (ODEs). It incorporates logistic growth to account for cell recovery and proliferation, and models a 3-day delay in fusion-induced death to reflect the syncytia formation lag phase. The syncytia model utilizes saturable kinetics to reflect receptor-mediated fusion dynamics and includes degradation of syncytia over time. Despite these improvements, several limitations remain. Both models assume homogeneous mixing of cells, constant per-cell expression of SP and ACE2, and binary interactions between fusion partners. Spatial heterogeneity, variable expression levels, and other complex TME factors are not considered. CV cells are treated as inert and excluded from interaction dynamics. Additionally, the fusion rate (k_f), degradation rate (k_{deg}), Michaelis-Menten constant (K_m), and delay time were derived from SARS-CoV-2 and HeLa cell literature rather than GBM-specific systems, which may limit biological relevance. Immune responses, such as cytokine signaling or immune cell recruitment, are not modeled. Future work will require expanded datasets, improved parameter fitting, and possibly multi-scale modeling approaches to better capture the complexity of GBM tumor-immune interactions.

Future Work

For the *in vitro* model, the next immediate step would be to engineer stable cell lines in an additional human GBM cell line. There were difficulties engineering the LVs in the U87 human GBM line, which may require repeating a kill curve to determine the puromycin concentration needed to eliminate non-transduced cells. Once established, the experimental setup described above could be applied to this or another human GBM cell line to validate findings and increase clinical relevance.

Cytokine profiling of the syncytia-forming GBM cultures would also be a valuable next step. Following fusogenic activity induced by SP and ACE2 expression, cytokine and chemokine release could be measured using an ELISA or a Western blot. Quantifying pro-inflammatory cytokines (e.g., IL-6, TNF-α), interferons (e.g., IFN-γ), and chemokines (e.g.,

CXCL10) would provide insight into immune activation. In addition, measuring PD-L1 expression in these cells could assess whether the fusogenic response induces compensatory immune checkpoint upregulation, which may influence the tumor's ability to evade immune attack. This could be evaluated using Western blot, qPCR, or flow cytometry. Quantifying the extent of syncytia formation (e.g., number and size per field of view) and correlating it with cell viability will help determine the lethality of the fusion events. Image analysis tools or high-content screening may be used to support this assessment. Since SP and ACE2 expression are controlled by doxycycline, this system also allows for tunable immune activation. Future experiments could turn expression on or off to study the dynamics of immune priming, suppression, or exhaustion over time. Collectively, these analyses would help characterize the immune landscape following syncytia formation and inform potential combination strategies with immunotherapies such as checkpoint inhibitors. Moreover, a valuable next step would be to test the fusogenic system in combination with existing GBM treatments, such as chemotherapy (e.g., temozolomide) or immune checkpoint inhibitors (e.g., anti-PD-1). Co-treating syncytia-forming cultures with checkpoint inhibitors could enhance immune activation, increase T cell activity, and reduce tumor cell survival. Similarly, combining fusogenic therapy with a chemotherapeutic agent like temozolomide may reveal whether this approach can complement or improve standard-of-care treatments. These experiments would provide early translational insight into how fusogenic therapies could be integrated into combinatorial treatment strategies for GBM.

In future studies, this fusogenic system could be tested *in vivo* using a murine model with subcutaneous or orthotopic GBM tumors to evaluate the effects of SP expression and doxycycline cycling on immune activation and tumor progression. Measuring additional immune signals as endpoints would improve the rigor and translational relevance of the model. Cytokine profiling, T cell activation assays, and analysis of tumor-infiltrating immune cells such as CD8+ T cells, CD4+ T cells, macrophages, and NK cells would provide deeper insight into the immune response induced by SP expression. Flow cytometry and immunohistochemistry could help identify the specific populations involved and assess their functional status. Monitoring tumor growth over time using serial imaging of both SP-expressing and control tumors would allow for the quantification of the therapeutic response. Incorporating immune checkpoint markers such as PD-L1 into the analysis would offer a more comprehensive understanding of how fusogenic therapy engages and modulates the immune system. Since SP expression is controlled by doxycycline, this system would enable inducible immune activation and could be used to test timing-dependent therapeutic windows. Future development should also explore long-term delivery vehicles, such as LVs with sustained expression or implantable doxycycline-release systems, to support durable immune engagement *in vivo*.

Future versions of the computational model could incorporate tumor volume as a dependent variable, allowing for more direct predictions of therapeutic efficacy. Collecting and integrating temporal *in vitro* data, such as longitudinal viability, fusion, or fluorescence measurements, would support more accurate parameter fitting and validation. Expanding the model to include interactions with immune cells or therapeutic antibodies could simulate the effects of immune engagement or checkpoint modulation in response to fusion-based therapies. In the model, a fixed delay is implemented using a time-based threshold to approximate the lag between syncytia formation

and GBM cell death. Future iterations could incorporate a distributed delay differential equation (DDE) to better represent variability in apoptotic or immune activation timing, particularly for modeling secondary immune responses. Since this model is based on an *in vitro* system using engineered U251 GBM cells, future work should explore how the system behaves *in vivo* and in human clinical contexts. Modeling tumor behavior within more complex environments would provide stronger translational value. Additionally, simulating custom doxycycline induction schedules could help optimize treatment timing by identifying regimens that maximize tumor cell killing while minimizing syncytia degradation, immune exhaustion, and/or off-target effects.

Materials and Methods

In Vitro Preparation

Before *in vitro* experimentation, an adherent cell culture protocol for Dr. Purow's lab was followed to grow GBM U251 cells. This consisted of first thawing the frozen vials of GBM U251 cells retrieved from the liquid nitrogen tank and then using the centrifuge to spin the cells down into a cell pellet. After centrifugation, the supernatant was carefully aspirated from above the cell pellet, and the pellet was resuspended in Roswell Park Memorial Institute (RPMI) media and transferred into a T-75 flask. The flask was placed in a cell culture incubator set at 37 °C and at a 5% CO_2 concentration to allow for cell growth. Cell growth was monitored daily via microscopy, and RPMI media was changed every 2–3 days. When the cells reached 80–90% confluency, the cells were subcultured using trypsin. After this process, the cells were considered ready for lentiviral transduction, though they required continuous monitoring and culture maintenance to remain viable for future use. Cell culture protocols were also followed for human GBM U87 cells; however, these cells were not conducive for lentiviral transduction. Therefore, the analysis was only performed on GBM U251 cells.

For successful lentiviral transduction, it was important to first conduct a kill curve experiment on GBM U251 cells using puromycin, an antibiotic. This was done by following the kill curve protocol for Dr. Purow's lab. A kill curve experiment was necessary to determine the minimum puromycin concentration that would kill all of the GBM U251 cells. Once determined, lentiviral transduction could take place by growing cells in RPMI media that contain puromycin at that optimal concentration. Leveraging the lentiviral transduction protocol and LV particles from OriGene, GBM U251 cells were plated in 24-well plates, with three wells assigned to each LV type (SP, ACE2, SP+ACE2, or CV). After a week of puromycin selection, wells that still showed cell proliferation were lifted with trypsin and transferred to T-25 flasks. These cells were considered stably transduced. Once the stable lines reached high confluence in the T-25s, they were further expanded into T-75 flasks to allow for large-scale culture. Each LV included a puromycin resistance gene, allowing only GBM U251 cells that successfully incorporated the LV to survive. This enabled selective growth of stably transduced cell lines, while non-transduced cells were eliminated by puromycin treatment. These flasks were monitored over a week to allow for lentiviral transduction to occur. They were then subcultured and continuously maintained as unique stable cell constructs of GBM U251 cells. These methods can be seen in *Figure S1*.

In Vitro Assays

Cell Viability Assays

The first cell viability assay conducted was a Nano-Glo® luciferase killing assay. This assay was used with the parental mouse cell line CT2A and human GBM U251-luciferase cells.

There were three different CT2A cell groups, including engineered CT2A-SP H3 cells, engineered CT2A-SP H6 cells, and parental CT2A cells not expressing SP. CT2A-SP H3 and CT2A-SP H6 represent two different SP-expressing cell subtypes. The human GBM U251-luciferase cells were leveraged as the target metric for this experiment. The goal of this viability assay was to determine if the CT2A-SP cell environments resulted in more human GBM U251-luciferase cell death than the parental CT2A cell environments, which did not express SP. Using the Nano-Glo® luciferase killing assay protocol for Dr. Purow's lab, cells were seeded into two 96-well plates. CT2A-SP H3 cells and U251-luciferase cells were seeded in one 96-well plate in replicates of five for varying ratios of CT2A-SP H3 cells to human GBM U251-luciferase cells. These varying ratios included 4:1, 2:1, 1:1, 1:2, and 1:1 (with no doxycycline in the final row), with SP-expressing cells represented as the left number and the luciferase cells represented as the right number. On the other half of the same 96-well plate, parental CT2A cells were also combined with U251-luciferase cells in replicates of five for the same varying ratios. This would serve as a control group for comparison with CT2A-SP H3 cells. The same setup was done on the other 96-well plate, but used CT2A-SP H6 cells instead of CT2A-SP H3 cells. After cell seeding, the plates were put in the incubator. Two days later, doxycycline, which is an antibiotic that can induce SP expression, was added to every row of the two 96-well plates except the 1:1 (no doxycycline) rows. The plates were then returned to the incubator for another five days. At the end of the five-day period, the lysis buffer was added to the plates, enabling luminescence readings of the targeted human U251-luciferase cells to be recorded upon placement into the plate reader.

The second Nano-Glo® luciferase killing assay was completed with human U251-luciferase cells and engineered human GBM U251 cell constructs. These stable cell constructs included U251 cells expressing SP, SP and ACE2, and CV. The goal of this viability assay was to determine if the U251-SP cell environment and the U251-SP+ACE2 cell environment led to more human GBM U251-luciferase cell death than the human GBM U251-CV cell environment, which did not express a viral protein. In a very similar setup to the first viability assay, cells were seeded into two 96-well plates. One 96-well plate had four rows of varying ratios of GBM U251 cells expressing SP to U251 luciferase cells. These cell ratios consisted of concentrations in combinations of 4:1, 2:1, 1:1, and 1:2, with SP cells representing the left number and luciferase cells representing the right number. There were five replicates in each row. On the other side of the same 96-well plate, U251 cells expressing CV were also combined with human U251-luciferase cells in replicates of five for the same varying ratios. The same setup was done on the other 96-well plate, but with U251 cells expressing SP and ACE2 instead of U251 cells expressing only SP. After cell seeding, the plates were put in the incubator for seven days. After incubation, a lysis buffer was added to the plates to enable luminescence reading upon placement in the plate reader. These methods can be seen in *Figure S2*.

Fluorescence Assay

The first step of the fluorescence assay was to perform an 8-well chamber slide experiment with our stable U251 cell constructs. The setup included one chamber with stable U251-ACE2 cells, one chamber with U251-SP cells, two chambers with U251-SP+ACE2 cells, and four chambers with varying ratios of U251-SP cells to U251-ACE2 cells. The ratios included combinations of 4:1, 2:1, 1:1, and 1:2 with stable U251 SP expressing cells representing the first number and stable U251

ACE2 expressing cells representing the second number. After seeding the cells, the 8-well chamber was placed in the incubator for six days. After incubation, 4',6-diamidino-2-phenylindole (DAPI) staining was applied to each chamber, and fluorescence non-inverted microscopy was performed. Fluorescence images at 40X magnification were taken with DAPI staining visualized as blue and representative of the cell nuclei, RFP staining visualized as red and representative of SP LV uptake within the cells, and GFP staining visualized as green and representative of ACE2 LV uptake within the cells. Fluorescence images were also taken to visualize the overlay of all the stains, and appeared as a color mixture of red, blue, and green together. Beyond visualization of the nuclei, SP LV cell uptake, and ACE2 LV cell uptake, syncytia formation was additionally observed and imaged as regions of multinucleated giant cells. These methods can be seen in *Figure S2*.

Statistical Analysis

Statistical tests were performed only on the cell viability assays and were not needed for the fluorescence assay, which sought only qualitative observations. For the first cell viability assay done with CT2A cells, the statistical tests used were two-tailed unpaired t-tests. For each ratio, this test was conducted to assess the statistical significance of luminescence differences between U251-luciferase cells in a CT2A-SP cell environment and those in a parental CT2A non-expressing SP cell environment. This statistical analysis was conducted in Excel by first averaging the replicates for each ratio and calculating the standard deviation. Two-tailed unpaired t-tests were then performed in Excel to compare the averages of SP-expressing and non-expressing conditions at each ratio. The same statistical approach was applied to the second cell viability assay using U251 cell constructs to compare luminescence between SP-expressing or SP+ACE2-expressing environments and control vector (CV) environments. Statistical significance was evaluated at a 95% confidence level ($p \leq 0.05$). One-tailed unpaired t-tests could also have been used in statistical analysis since the goal was to determine whether luminescence was lower in SP-expressing or SP+ACE2-expressing environments compared to non-expressing environments. However, due to uncertainty regarding whether treatment groups would show an increase or decrease in luminescence across both cell viability assays, two-tailed unpaired t-tests were seen to be the better option.

Predictive Logistic Growth Models

After conducting the *in vitro* assays, two analytical computational models were created for both cell viability and syncytia formation. The predictive cell viability model is directly related to the Nano-Glo® luciferase killing assay, but it is on a more controlled and simplified experimental setup than was used previously. The model setup assumes that the initial total cell count remains the same across groups, while the ratios of cells expressing SP, ACE2, and CV vary between different groups. Additionally, the initial count of GBM U251-luciferase cells is kept constant across groups. Although syncytia formation is not the direct metric of measurement for the Nano-Glo® luciferase killing assay, it is a contributing factor to cell viability. Therefore, it was important to create a predictive syncytia model alongside the cell viability model to broaden understanding of the experiment.

The predictive cell viability model took into account various parameters in its development, including SP consumption, ACE2 consumption, and U251-luciferase cell death. Since these parameters change over time due to syncytia formation, they can all be represented as ODEs seen in *Equation S1*. These parameters

are captured in the equations with time denoted as t, SP denoted as S, ACE2 denoted as A, the syncytia formation rate denoted as k_f, and GBM U251-luciferase cell death denoted as D. The total initial count of U251-luciferase cells was set to 120 (U_0), and a maximum carrying capacity (K) of 1000 cells was defined to account for growth constraints. These equations were created based on a few assumptions. The first assumption was that SP consumption, ACE2 consumption, and U251-luciferase cell death are all dependent on syncytia events and therefore rely on a specific syncytia formation rate (k_f). Based on previous literature, a rough estimation for k_f within our experiment was determined to be approximately $5 \times 10^{-4}\ hr^{-1}$.[24] The second assumption was that for each syncytial event, there will be a decrease in S due to SP consumption and a decrease in A due to ACE2 consumption. The third assumption was that for each syncytial event, there would be a doubling in GBM U251-luciferase cell death (D). Another key assumption was that GBM U251-luciferase cell death due to syncytia formation would begin after a 3-day delay, which was implemented in the model using a conditional time-based term.[25] It was also assumed that U251-luciferase cells proliferate according to a defined growth rate (r).[21] This growth rate was estimated to be around 0.1 $\frac{luciferase\ cells}{hr}$. Lastly, it was assumed that U251-luciferase cell viability would be best represented by a modified logistic growth model that takes into account all the above assumptions. This model combines proliferation and fusion-induced cell death by incorporating a delay condition that activates syncytia-related death after the third day. The x-axis of the plotted model represents time in days spanning over a seven-day period to allow for syncytia-induced U251-luciferase cell death to occur. The y-axis of the plotted model represents cell viability as a percentage of the initial seeded number of U251-luciferase cells. There were five SP:ACE2:CV ratio conditions superimposed on the plotted model, including ratios of 6:2:0, 4:4:0, 4:2:2, 2:4:2, and 2:2:4.

The predictive syncytia model builds upon the same parameters used in the cell viability model with the addition of a new cell fusion parameter, denoted as F. F represents the number of syncytia, or multinucleated fused cells, formed through interactions between SP-expressing and ACE2-expressing U251 GBM cells. This model leveraged the same differential equations seen in *Equation S1*, with the inclusion of the syncytia formation differential equation, shown in *Equation S2*. In addition to the new variable F, a degradation rate constant for syncytia (k_{deg}) was introduced. Most of the assumptions used in the cell viability model apply in this model. However, this model assumes there is no time delay in syncytia formation, as fusion begins as soon as cells are seeded. Another key assumption is that syncytia are not permanent and will degrade over time. Based on the literature, it was determined that this degradation rate was approximately 0.0735 $\frac{cell\ fusions}{hr}$.[26] Fusion was modeled using a saturable reaction term to capture the biological constraint of limited fusion partners. The plotted model has the same x-axis, y-axis, and superimposed ratio conditions. This model provides insight into the kinetics of syncytia formation across experimental conditions and serves as a predictive tool for understanding how SP:ACE2:CV ratios influence fusion behavior.

End Matter

Author Contributions and Notes

K.S., B.L., and F.W. created the ODE computational model, completed experimental data analysis with the ODE equations, and developed an analytical ODE model. B.P. advised the creation of the analytical ODE model and experimental analysis. K.S., B.L., A.H., and F.W. conducted *in vitro* experiments,

obtained experimental data, l, and performed statistical analysis. K.S., B.L., A.H., and F.W. wrote the report. B.P. read and provided edits for the report. The authors declare no conflict of interest.

Acknowledgments

We would like to thank Benjamin Purow M.D, Yunge Zhao Ph.D, and Timothy Allen Ph.D for their contributions, support, and guidance.

Supplemental Figures

A.

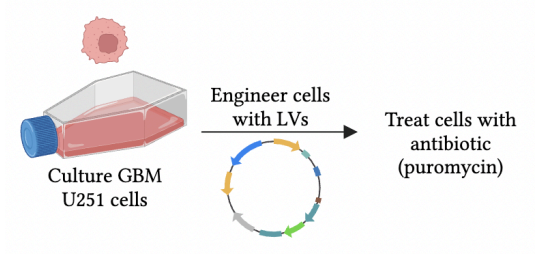

B.

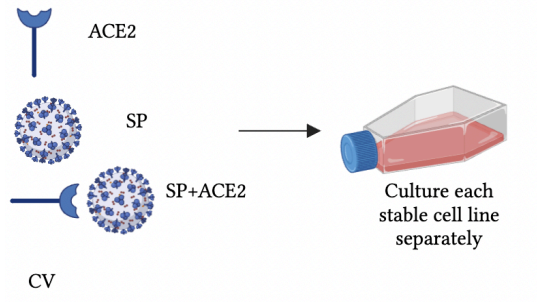

Figure S1. Engineering GBM U251 cells with LVs expressing ACE2, SP, SP+ACE2, or a CV, followed by puromycin selection and stable cell line culture.
(A) U251 GBM cells were cultured and transduced with lentiviral vectors encoding either SARS-CoV-2 SP, the ACE2 receptor, both SP and ACE2, or a CV. Cells were then treated with puromycin for antibiotic selection.
(B) Stably transduced U251 lines were expanded and cultured separately to generate four engineered cell lines (SP, ACE2, SP+ACE2, and CV). These cell lines served as the basis for downstream assays assessing cytotoxicity, fusion dynamics, and therapeutic potential.

A.

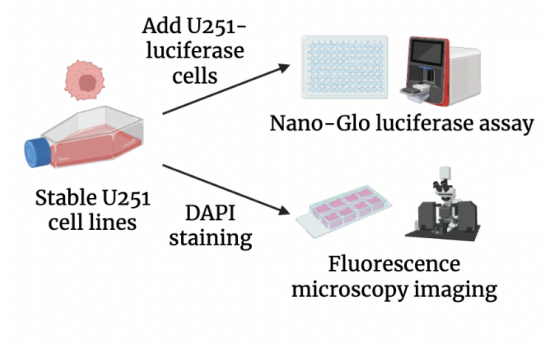

B.

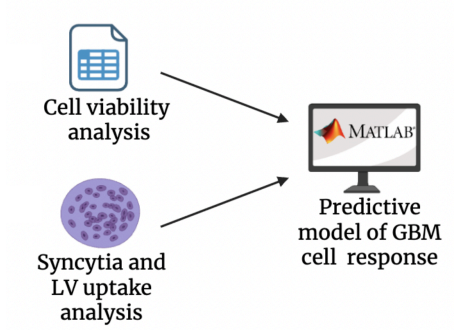

Figure S2. *In vitro* evaluation of fusogenic lentiviral constructs using U251 stable cell lines.
(A) Stable U251 cell lines were co-cultured with U251-luciferase cells to assess fusion-mediated cytotoxicity. Cell viability was quantified using the Nano-Glo luciferase assay, and syncytia formation was visualized via DAPI staining and non-inverted fluorescence microscopy.
(B) Quantitative cell viability and imaging data were used for downstream analysis and integrated into a MATLAB-based computational model simulating GBM cell response. This platform enabled functional evaluation of fusion-induced cell death and predictive modeling of syncytia kinetics.

Supplemental Equations

A.

$$\frac{dS}{dt} = -\ kfS(t)A(t)$$

B.

$$\frac{dA}{dt} = -\ kfS(t)A(t)$$

C.

$$\frac{dD}{dt} = 2kfS(t)A(t)$$

Equations S1. SP consumption is represented by the differential equation noted by **(A)**, ACE2 consumption is represented by the differential equation noted by **(B)**, and U251-luciferase cell death is represented by the differential equation noted by **(C)**.

A.

$$\frac{dF}{dt} = -\ kfS(t)A(t)\ -\ kdegF(t)$$

Equations S2. Cell fusions are represented by the differential equation noted by **(A)**.

References

1. Thakkar JP. Glioblastoma Multiforme. AANS. April 15, 2024. Accessed September 8, 2024. https://www.aans.org/patients/conditions-treatments/glioblastoma-multiforme/

2. Tamimi AF, Juweid M. Epidemiology and Outcome of Glioblastoma. In: De Vleeschouwer S, ed. *Glioblastoma*. Codon Publications; 2017. Accessed September 24, 2024. http://www.ncbi.nlm.nih.gov/books/NBK470003/

3. Tamimi AF, Juweid M. Epidemiology and Outcome of Glioblastoma. In: De Vleeschouwer S, ed. *Glioblastoma*. Codon Publications; 2017. Accessed November 12, 2024. http://www.ncbi.nlm.nih.gov/books/NBK470003/

4. Ståhl P, Henoch I, Smits A, Rydenhag B, Ozanne A. Quality of life in patients with glioblastoma and their relatives. *Acta Neurol Scand*. 2022;146(1):82-91. doi:10.1111/ane.13625

5. Glioblastoma (GBM): What It Is, Causes, Symptoms & Prognosis. Accessed September 8, 2024. https://my.clevelandclinic.org/health/diseases/17032-glioblastoma

6. Glioblastoma Multiforme | Cedars-Sinai. Accessed September 8, 2024. https://www.cedars-sinai.org/health-library/diseases-and-conditions/g/glioblastoma-multiforme.html

7. Davis ME. Glioblastoma: Overview of Disease and Treatment. *Clinical journal of oncology nursing*. 2016;20(5):S2. doi:10.1188/16.CJON.S1.2-8

8. Monitoring and optimizing cognitive function in cancer patients: Present knowledge and future directions - PMC. Accessed November 12, 2024. https://pmc.ncbi.nlm.nih.gov/articles/PMC4250534/

9. Glioblastoma Multiforme. AANS. Accessed November 6, 2024. https://www.aans.org/patients/conditions-treatments/glioblastoma-multiforme/

10. Wesolowski JR, Rajdev P, Mukherji SK. Temozolomide (Temodar). *AJNR: American Journal of Neuroradiology*. 2010;31(8):1383. doi:10.3174/ajnr.A2170

11. Redmond KJ, Mehta M. Stereotactic Radiosurgery for Glioblastoma. *Cureus*. 2015;7(12):e413. doi:10.7759/cureus.413

12. Fernandes C, Costa A, Osório L, et al. Current Standards of Care in Glioblastoma Therapy. In: De Vleeschouwer S, ed. *Glioblastoma*. Codon Publications; 2017. Accessed November 6, 2024. http://www.ncbi.nlm.nih.gov/books/NBK469987/

13. Lentiviral Transduction of Primary Human Glioblastoma Cultures | SpringerLink. Accessed November 6, 2024. https://link.springer.com/protocol/10.1007/978-1-4939-7659-1_6

14. Hagemann C, Meyer C, Stojic J, et al. High efficiency transfection of glioma cell lines and primary cells for overexpression and RNAi experiments. *J Neurosci Methods*. 2006;156(1-2):194-202. doi:10.1016/j.jneumeth.2006.03.003

15. Vecchio CD, Calistri A, Parolin C, Mucignat-Caretta C. Lentiviral Vectors as Tools for the Study and Treatment of Glioblastoma. *Cancers*. 2019;11(3):417. doi:10.3390/cancers11030417

16. Miletic H, Fischer YH, Giroglou T, et al. Normal brain cells contribute to the bystander effect in suicide gene therapy of malignant glioma. *Clin Cancer Res*. 2007;13(22 Pt 1):6761-6768. doi:10.1158/1078-0432.CCR-07-1240

17. Willson CM, Lequio M, Zhu Z, et al. The Role of SARS-CoV-2 Spike Protein in the Growth of Cervical Cancer Cells. *Anticancer Res*. 2024;44(5):1807-1815. doi:10.21873/anticanres.16982

18. Johnson BD, Zhu Z, Lequio M, et al. SARS-CoV-2 spike protein inhibits growth of prostate cancer: a potential role of the COVID-19 vaccine killing two birds with one stone. *Medical Oncology (Northwood, London, England)*. 2022;39(3):32. doi:10.1007/s12032-021-01628-1

20. Burton C, Bartee E. Syncytia Formation in Oncolytic Virotherapy. Mol Ther Oncolytics. 2019;15:131-139. doi:10.1016/j.omto.2019.09.006

21. Do M, Kwak IH, Ahn JH, Lee IJ, Lee JH. Survivin protects fused cancer cells from cell death. *BMB Rep*. 2017;50(7):361-366. doi:10.5483/BMBRep.2017.50.7.185

22. Davis ME. Glioblastoma: Overview of Disease and Treatment. *Clinical journal of oncology nursing*. 2016;20(5):S2. doi:10.1188/16.CJON.S1.2-8

23. Tomaszewski W, Sanchez-Perez L, Gajewski TF, Sampson JH. Brain Tumor Micro-Environment and Host State — Implications for Immunotherapy. *Clin Cancer Res*. 2019;25(14):4202-4210. doi:10.1158/1078-0432.CCR-18-1627

24. Amidei, Ava, and Hana M Dobrovolny. "Estimation of virus-mediated cell fusion rate of SARS-CoV-2." *Virology* vol. 575 (2022): 91-100. https://doi.org/10.1016/j.virol.2022.08.016

25. Giesker K, Hensel M. Bacterial Vaccines. In: *Reference Module in Biomedical Sciences*. Elsevier; 2014. doi:10.1016/B978-0-12-801238-3.00141-0

26. Jessie, B., & Dobrovolny, H. M. (2021). The role of syncytia during viral infections. *Journal of theoretical biology*, *525*, 110749. https://doi.org/10.1016/j.jtbi.2021.110749